1 Orbit control applications

Content

1.1 Objectives

1.2 Drag-free control

1.2.1 Concept and aims

Drag-free control allows a body to move continuously only subject to local gravity: free fall. Two main implementations are possible, which may mix each other.

1) Proof-mass concept: a tiny body (proof-mass, < 1 kg) is free to move inside a cage on a spacecraft, thus 'ideally' free from any non-gravitational force. The spacecraft is actuated to keep the mass centered and aligned to the cage upon measurement of relative position and attitude: in other words the satellite tracks the proof-mass. Contact between cage and proof-mass destroys free-fall, implying sensors to be contactless (capacitive sensors). The concept dates back to 1960 when U.S. DISCOS was successfully launched and operated [1]. Of course, a satellite tracking a drag-free body tends to become drag-free. The concept has several difficulties, owing to the oddity that a large mass body (> 1000 kg) is made tracking a small mass body! In addition, only a single proof-mass per spacecraft can be made drag-free.
2) Accelerometer concept: the whole satellite is made drag-free upon direct measurement and compensation of the non-gravitational forces (aerodynamic forces, solar pressure, …). In this way, any free body inside the spacecraft would 'ideally' float (free fall) as the astronauts in the International Space Station[1]. Actually, proof-masses on board of drag-free satellite are not left free (they would drift because of parasitic forces), but are actively suspended to be used as 3D accelerometers (see Chapter 3). Now several proof-masses may be employed: GOCE (Gravity field and steady-state Ocean Circulation Explorer) mounts a 3D ultra-sensible gradiometer consisting of six accelerometers at the vertices of an octahedron. A similar concept is employed since 1959 by U.S. NASA (National Aeronautics and Space Administration) and later by European Space Agency in the so-called 'Vomit Comets' ('free falling' aircrafts) for training astronauts to weightlessness. Such aircrafts may repeat several 25s near-parabolic flights (actually cycloid profiles in altitude) in which propulsion and steering are actuated to cancel drag and lift [2].

[1] The International Space Station is not exactly drag-free (speak of microgravity) as the orbit decays of about 2 km/month because of thermosphere drag at the mean altitude of 350 km. This obliges orbit raising maneuver to be done several times each year depending on thermosphere density.

To understand how drag-free satellites may be employed for scientific purposes, two basic principles must be recalled and formulated.

1) Galileo equivalence principle: acceleration of free-falling bodies, in a uniform gravity field, is independent of inertial mass m and composition. To this end, write the gravity acceleration as the gradient of a gravity potential $U(\vec{\mathbf{r}})$ (Chapter 1, 1.96) times the gravitational mass $m_g = k_m m$, where k_m is a universal constant set conventionally to unit. Writing free-fall equation as follows

$$\dot{\vec{\mathbf{v}}}(t) = \vec{\mathbf{g}}(\vec{\mathbf{r}}, t, k_m) = k_m \nabla U(\vec{\mathbf{r}}, t), \tag{7.1}$$

Galileo principle amounts to $k_m = \text{constant} = 1$, an assumption underlying Chapter 1. Figure 1 shows astronaut Dave Scott on the Moon, 1971, before dropping a hammer (left) and a feather (right). The objects hit moon dust at the same instant. "Mr. Galileo was right" he exclaimed.

Figure 1. Astronaut Dave Scott on the Moon, 1971.

2) Einstein (weak) equivalence principle: starting from Galileo principle, Einstein suggested free-falling bodies are 'local' inertial frames, where Newton's equation holds. In other terms, gravitational acceleration has no local dynamical effects. Indeed, also in a non-uniform gravity field as soon as two bodies approach, their differential acceleration goes to zero. Were Galileo principle false, the same occurred to Einstein's. Consider two bodies

$$\begin{aligned} \dot{\vec{\mathbf{v}}}_0(t) &= k_{m0} \nabla U(\vec{\mathbf{r}}_0, t) \\ \dot{\vec{\mathbf{v}}}_1(t) &= k_{m1} \nabla U(\vec{\mathbf{r}}_1, t) \end{aligned}, \tag{7.2}$$

where $k_{mj} = m_{gj} / m_j$, $j = 0,1$. Making bodies to become closer, i.e. $\vec{\mathbf{r}}_1 \to \vec{\mathbf{r}}_0 \to \vec{\mathbf{r}}$, leads to

$$\lim_{\vec{\mathbf{r}}_1 \to \vec{\mathbf{r}}_0} \left(\dot{\vec{\mathbf{v}}}_1(t) - \dot{\vec{\mathbf{v}}}_0(t) \right) = (k_{m1} - k_{m0}) \nabla U(\vec{\mathbf{r}}, t), \tag{7.3}$$

that goes to zero under Galileo principle $k_{m0} = k_{m1}$ [1]. Time evolution of the relative position $\Delta\vec{\mathbf{r}}(t) = \vec{\mathbf{r}}_1(t) - \vec{\mathbf{r}}_0(t)$ is an (unbounded) free response driven by initial conditions

$$\Delta\vec{\mathbf{r}}(t) = \Delta\vec{\mathbf{r}}(t_0) + \Delta\vec{\mathbf{v}}(t_0)(t - t_0). \tag{7.4}$$

The bodies tend to separate like the hair of the astronaut Marsh Ivins in Figure 2.

Figure 2. Astronaut Marsha Ivins demonstrates weightlessness on long hair during Space Shuttle mission, 2001

Now assume body 1 is subject to a force $\vec{\mathbf{F}}_1$ (either internal or external), thus ceasing to be free-falling. Relative motion satisfies Newton's equation

$$\lim_{\vec{\mathbf{r}}_1 \to \vec{\mathbf{r}}_0} \left(\dot{\vec{\mathbf{v}}}_1(t) - \dot{\vec{\mathbf{v}}}_0(t) \right) = \vec{\mathbf{F}}_1 / m_1 . \tag{7.5}$$

3) When free-falling proof-masses become distant, they sense non uniform and irregular gravity potential, as Galileo principle leads to

$$\Delta\dot{\vec{\mathbf{v}}}(t) = \nabla U(\vec{\mathbf{r}}_1, t) - \nabla U(\vec{\mathbf{r}}_0, t) = \nabla^2 U(\vec{\mathbf{r}}_0, t)\, \Delta\vec{\mathbf{r}}(t) + \dots . \tag{7.6}$$

where $\Delta\dot{\vec{\mathbf{v}}}(t) = \dot{\vec{\mathbf{v}}}_1(t) - \dot{\vec{\mathbf{v}}}_0(t)$ and $\Delta\vec{\mathbf{r}}(t) = \vec{\mathbf{r}}_1(t) - \vec{\mathbf{r}}_0(t)$ are relative speed and position, $\nabla^2 U(\vec{\mathbf{r}}_0)$ is the so-called gravity tensor, and the relevant elastic force is the so-called tidal force, as tides occur because of this force. Tidal forces are responsible for ground and see tides on the Earth surface and for space events like the fragmentation of the comet in Figure 3.

---

[1] The quantity $\eta = 2|k_{m1} - k_{m0}| / (k_{m1} + k_{m0}) \cong |k_{m1} - k_{m0}|$ is called the Eötvös parameter and is known to be less than 10^{-12}. Several space missions aiming at testing η down to 10^{-17} are planned, since the equivalence principle is the cornerstone of the Einstein's general relativity.

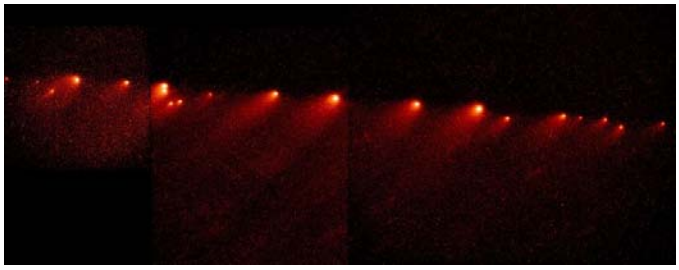

Figure 3. Comet Shoemaker-Levy fragments, 1994, after breaking up in 1992 under Jupiter's tidal forces

One of theories trying to explain the formation of the rings of Saturn (proposed by the French astronomer E. Roche in the 19th century, see below) is that rings are due to disintegration of a moon of Saturn that came too close to Saturn (below the Roche limit) to be ripped apart by tidal forces.

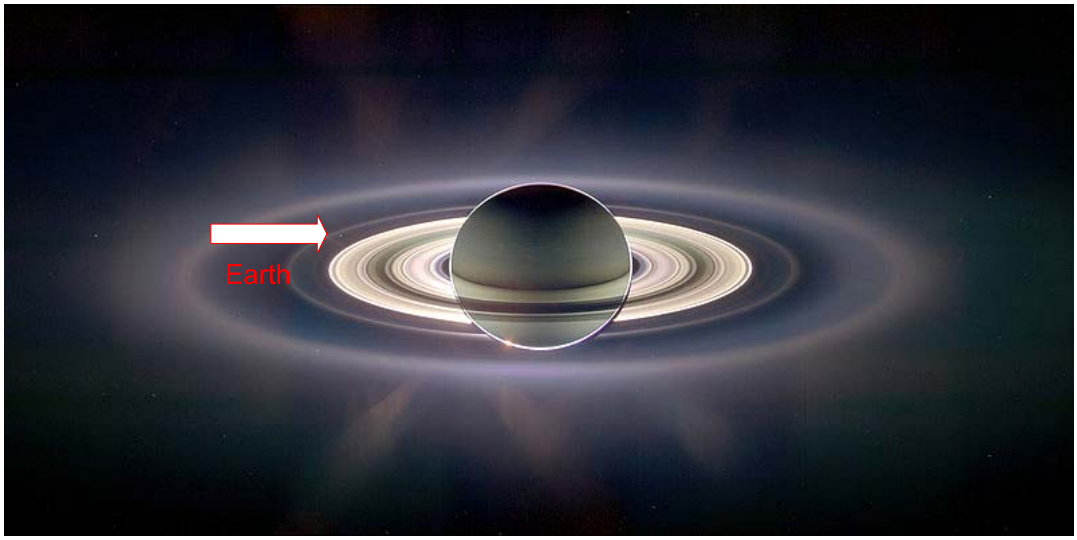

Figure 4. The rings as Saturn is eclipsing the Sun are imaged by the US-Europe Cassini spacecraft in 2006 (from Wikipedia, brightness is exaggerated). The arrow points to a pale spot corresponding to the Earth

Exercise 1. Consider a small body of radius r and density ρ (mass m) approaching a large body of density ρ_0 and radius r_0 (mass m_0) Which is the limit distance d_{Roche} below which the small body will disintegrate? It is called the Roche limit from a French astronomer that first computed it.

Solution. Consider a test mass μ on the small body surface on the face toward the large body. The acceleration of the test mass is

$$\dot{w} = \frac{Gm}{r^2} - \frac{Gm_0}{(d-r)^2} \cong \frac{Gm}{r^2} - \frac{Gm_0}{d^2} - \frac{2Gm_0 r}{d^3}, \tag{7.7}$$

where the last term is the tidal acceleration due to non uniform gravity. The acceleration of the small body is

$$\dot{v} = -\frac{Gm_0}{d^2}. \tag{7.8}$$

The relative acceleration of the test mass with respect to the small body is

$$\dot{w} - \dot{v} = Gr\left(\frac{m}{r^3} - \frac{2m_0}{d^3}\right) = \frac{4\pi Gr}{3}\left(\rho - \frac{2\rho_0 r_0^3}{d^3}\right). \tag{7.9}$$

Until the bracket term in (7.9) is non negative the test mass is attracted by the small body, on the contrary it will move toward the large body favouring disintegration. Zero acceleration provides the Roche limit

$$\frac{d_{Roche}}{r_0} = \left(\frac{2\rho_0}{\rho}\right)^{1/3}. \tag{7.10}$$

Compute the Roche limit for a comet with $\rho \approx 500$ kg/m^3 approaching the Earth ($\rho_0 \cong 5500$ kg/m^3).

Gravimetric missions aim to monitor gravity space/time irregularities by measuring tidal forces either from differential accelerations (gradiometer, on a single satellite, like GOCE, see Figure 4) or from relative position fluctuations (two or more distant satellites through radio waves , like GRACE, or optical interferometry). Making proof-masses distant, tidal forces increase and facilitate their measurement. Errors come from instruments and the residual non gravitational accelerations adding to (7.6). Drag-free control is therefore essential.

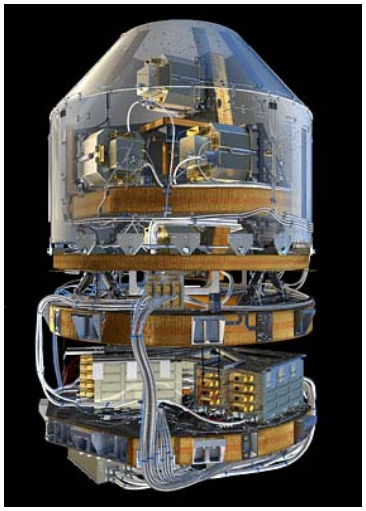

Figure 5. The GOCE gradiometer.

1.2.2 Control requirements

Consider a single spacecraft, and the dynamic equation as in Chapter 3,

$$\dot{\mathbf{v}}(t)=\mathbf{g}\left(\mathbf{r}(t)\right)+\frac{R_b(\boldsymbol{q})\left(-\mathbf{F}_d(t)+\mathbf{F}_t(t)\right)}{m},\ \mathbf{v}(0)=\mathbf{v}_0, \tag{7.11}$$

where $\mathbf{F}_d$ are environment non-gravitational forces (mainly aerodynamic at low-Earth orbit) and $\mathbf{F}_t$ are command forces due to a thrusters assembly. Both vectors are in body coordinates. Ideal drag-free requirement is

$$\mathbf{a}(t)=\left(-\mathbf{F}_d(t)+\mathbf{F}_t(t)\right)/m=0. \tag{7.12}$$

Actually requirements express a statistical performance of the residual non gravitational acceleration $\mathbf{a}$ in (7.12). To provide an example, restrict to the Earth gravity, whose potential has been defined in Chapter 1 as a function of polar Earth-fixed coordinates (r,λ,L)

$$U=\frac{\mu}{r}\left(1-\sum_{k=1}^{\infty}J_k\left(\frac{r_{\max}}{r}\right)^k P_k(\sin L)\right)+V(L,\lambda), \tag{7.13}$$

where L is the latitude and P_k is a Legendre polynomial of order k, depending on $\sin^k L$ and therefore on $\sin kL$, and corresponding to an Earth surface wavelength $\nu_k=2\pi R_E/k$.

Then consider a satellite in near-polar, $i\cong\pi/2$, near-circular orbit, $e\le 0.001$, whose inertial position may be approximated by

$$\mathbf{r}(t)\cong a\begin{bmatrix}\cos\Omega\cos(\omega+\underline{\omega}_O t)\\ \sin\Omega\cos(\omega+\underline{\omega}_O t)\\ \sin(\omega+\underline{\omega}_O t)\end{bmatrix}, \tag{7.14}$$

where Ω is the right-ascension of the ascending node, a the semi-major axis, ω the argument of perigee, that can be set to zero, and $\underline{\omega}_O$ the orbit angular frequency. Gravimetry aims to measure coefficients in (7.13) up to some order $k_{\max}$. By expressing $L=\underline{\omega}_O t$ and

$$2\pi f_k t=k\underline{\omega}_O t \tag{7.15}$$

the time frequency f_k corresponding to ν_k is $f_k=(2\pi)^{-1}k\underline{\omega}_O$. With $a=R_E+h$, $h=300$ km, $\underline{\omega}_O\cong 1.2$ mrad/s. Therefore $k_{\max}=500$, implies $f_{k,\max}\cong 0.1$ Hz. The variance of the residual acceleration is distributed in the frequency domain $f\le f_{k,\max}$ through an appropriate spectral density $\overline{S}_a^2(f)$, decreasing from lower to higher frequencies, since higher-order harmonics need more accuracy. In the case of GOCE the most demanding requirement covers the

frequency band $f_0 = 5$ mHz to $f_1 = 0.1$ Hz, asking $\bar{S}_a \le 0.02$ μm/s$^2/\sqrt{\text{Hz}}$, but extends above f_1 with a looser requirement, about 10 times higher.

1.2.3 Embedded Model

The design procedure stems from the model design, hereafter called Embedded Model (EM) as it is coded, as it is, in the control algorithms.

1.2.3.1 Controllable dynamics

It must describe command to measurement dynamics as well as disturbance dynamics. The former will be called controllable dynamics and in this case must account for thruster and accelerometer dynamics. Controllable dynamics must be as simple as possible, and must capture the high-frequency dynamics, close to the fastest disturbance components to be rejected, which in this case may cover $f_1 \le f \le f_{\max}$, where $f_{\max} = 0.5/T$ is the control Nyquist frequency to be designed. Since thruster and accelerometer BW are designed to be much larger than f_1, their dynamics may be greatly simplified. As a baseline we assume

1) accelerometer dynamics to be dominated by a delay $\tau_a \ge T$, to be accounted for by EM,
2) thruster dynamics to be dominated by a 1st order response with time constant $\tau_t \approx T$, to be neglected by EM.

As a consequence, a first-order dynamics for each axis results, where each axis should be distinguished by the subscript $k = x, y, z$, and all variables are in acceleration units, m/s^2,

$$\begin{aligned} x(i+1) &= (1-\beta)x(i) + \beta\left(d(i) + w_0(i) + u(i)\right) \\ y(i) &= x(i) + e(i) = y_m(i) + e(i) \end{aligned}, \tag{7.16}$$

where subscript k has been dropped for simplicity's sake.

In (7.16) the following variables and parameters have been used

1) $0 < \beta \le 1$ may be tuned to accelerometer and thruster dynamics, and specifically to a delay by $\beta = 1$,
2) $d = a_d + d_a$ is the sum of the non gravitational acceleration a_d to be rejected, and of the accelerometer drift and bias d_a, that cannot be separated from a_d, unless through calibration from a different instrument; w_0 is a white noise accounting for thruster noise,
3) $u = F_t / m$ is the commanded acceleration,
4) y is the accelerometer measurement corrupted by noise and model error e;
5) the total non gravitational acceleration affecting the spacecraft is

$$a = a_d + w_0 + u\,. \tag{7.17}$$

Axial dynamics is coupled through thruster matrix

$$\mathbf{F}_t = V_t \mathbf{u}_t \,. \tag{7.18}$$

1.2.3.2 Disturbance dynamics

The second part of EM is to fix the disturbance dynamics, so as to approximate in the high-frequency domain $f \geq f_1$ the disturbance spectral density. There disturbance is dominated by thruster (Figure 6) and accelerometer noise, to be treated as white noise w_u and e, and by short-term aerodynamic components, not very well known, but assumed to harmonically decrease with -40 dB/dec as in Figure 5, which implies the asymptotic spectral density of d

$$\begin{aligned} &\lim_{f\to\infty} S_d(f) = \underline{S}_d (f_d / f)^2 \\ &\lim_{f\to 0} S_d(f) = \underline{S}_d \end{aligned} \,. \tag{7.19}$$

Typical values at $h = 300$ km and high solar activity for the along-track component are

$$m\underline{S}_{dx} \leq 5 \text{ mN}/\sqrt{\text{Hz}},\ f_{dx} \cong 10 \text{ mHz}\,. \tag{7.20}$$

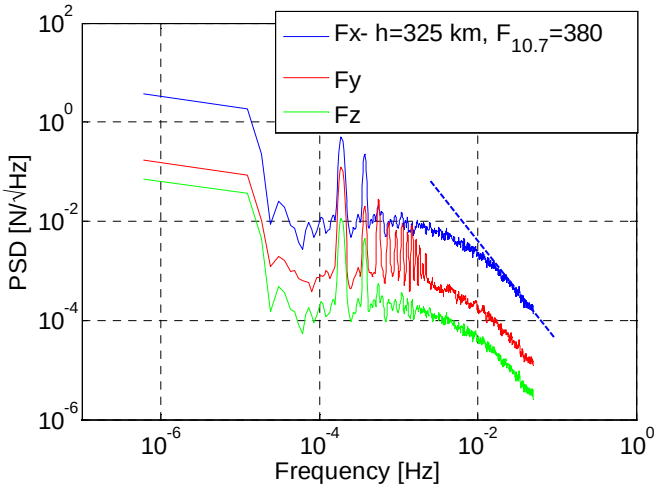

Figure 6. Simulated spectral density (unilateral root) of drag forces at an altitude of 325 km and the peak solar index of 380.

Figure 6 shows typical thruster noise of the mini ion-thruster adopted on GOCE. At $f_d = 10$ mHz the spectral density is much lower than the (along-track) aerodynamic density mS_{dx} in Figure 5. Thruster noise becomes significant for $f > 0.1$ Hz, where becomes flat and holds

$$S_t(f) \cong 0.02 \text{ mN}/\sqrt{\text{Hz}} \tag{7.21}$$

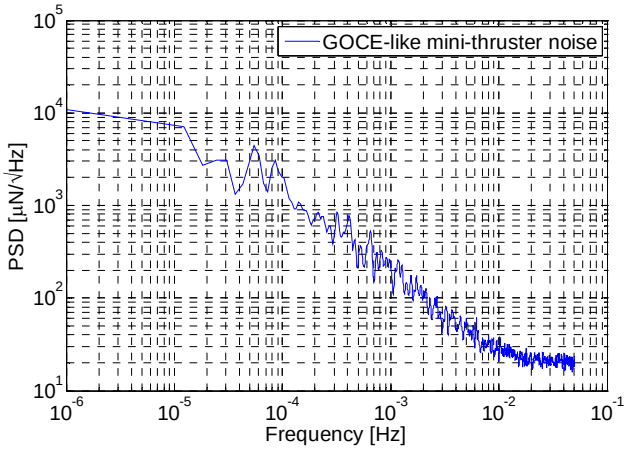

Figure 7. Simulated thruster noise of the GOCE type (ordinate in $\mu N/\sqrt{Hz}$).

2nd order spectral density implies a 2nd order dynamics including 1st and 2nd order random drift to be generic and therefore driven by a pair of white noise w_1, w_2. Denoting the relevant state variables with x_{d1}, x_{d2}

$$\begin{bmatrix} x_{d1} \\ x_{d2} \end{bmatrix}(i+1) = \begin{bmatrix} 1 & 1 \\ 0 & 1 \end{bmatrix}\begin{bmatrix} x_{d2} \\ x_{d2} \end{bmatrix}(i) + \begin{bmatrix} 1 & 0 \\ 0 & 1 \end{bmatrix}\begin{bmatrix} w_1 \\ w_2 \end{bmatrix}(i)$$
$$d(i) = \begin{bmatrix} 1 & 0 \end{bmatrix}\begin{bmatrix} x_{d2} \\ x_{d2} \end{bmatrix}(i) \qquad (7.22)$$

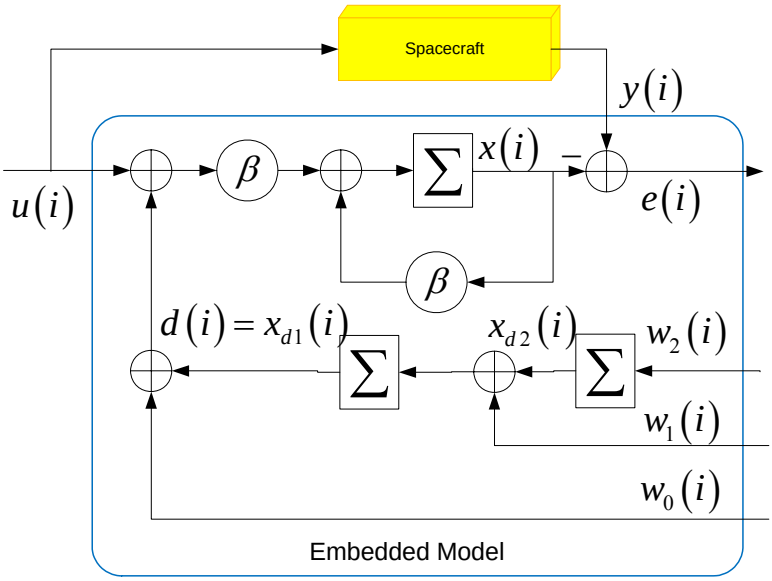

Figure 8. Embedded Model and model error.

1.2.4 Control architecture

1.2.4.1 Control law

By including the EM in the control algorithms, one immediately realizes the need of disposing each time iT of two input signals: the command $u(i)$ and the noise vector $\mathbf{w}(i)$,

$$\mathbf{w}(i) = \begin{bmatrix} w_0 \\ w_1 \\ w_2 \end{bmatrix}(i). \tag{7.23}$$

The command is computed by the control law, which in this case is very simple as must just cancel the disturbance d in (7.16)

$$u(i) = -d(i) = -x_d(i) \tag{7.24}$$

Remarks. Causality constraint. Note (7.24) cannot cancel w_0 in (7.16), since the latter cannot be predicted, being a white noise, whereas it will be shown below command must be always one-step predicted.

Remarks. Feedback control. One may wonder about (7.24) as it does not include a feedback component from the controllable state x in (7.16). Actually, controllable dynamics is asymptotically stable and the contribution of the unrejected noise w_0 is therefore bounded.

Remarks. Parasitic accelerometer drift. Note control law (7.24) cannot distinguish between aerodynamic component a_d and accelerometer drift d_a! The residual acceleration from (7.17) and (7.24), holds

$$a = w_0 - d_a . \tag{7.25}$$

1.2.4.2 Noise estimator and state predictor

Besides command, one must retrieve the noise vector. How? The following principles must be followed

1) noise is unpredictable and past independent, but encoded in past/present measurements once occurred,
2) the model error $e = y - y_m$ encodes the past noise effects not yet affecting the EM,
3) therefore the only noise source looks the model error signal.

The simplest way is a linear output-to-noise feedback

$$\mathbf{w}(i) = Le(i) = L\big(y(i) - x(i)\big)$$
$$L = \begin{bmatrix} l_0 \\ l_1 \\ l_2 \end{bmatrix} \quad . \tag{7.26}$$

Equations (7.26), (7.16) and (7.22) become a closed-loop state predictor, to be indicated with a different notation as the input noise is plant dependent through (7.26)

$$\begin{bmatrix} \hat{x} \\ \hat{x}_{d1} \\ \hat{x}_{d2} \end{bmatrix}(i+1) = \begin{bmatrix} 1-\beta-\beta l_0 & \beta & 0 \\ -l_1 & 1 & 1 \\ -l_2 & 0 & 1 \end{bmatrix} \begin{bmatrix} \hat{x} \\ \hat{x}_{d1} \\ \hat{x}_{d2} \end{bmatrix}(i) + \begin{bmatrix} \beta \\ 0 \\ 0 \end{bmatrix} u(i) + \begin{bmatrix} \beta l_0 \\ l_1 \\ l_2 \end{bmatrix} y(i)$$
$$\hat{y}_m(i) = \begin{bmatrix} 1 & 0 & 0 \end{bmatrix} \begin{bmatrix} \hat{x} \\ \hat{x}_{d1} \\ \hat{x}_{d2} \end{bmatrix}(i) \quad . \tag{7.27}$$

Specifically the 'hat' notation stands for one-step prediction as $\hat{x}(i+1)$ has been obtained from past $y(i)$, an alternative, heavier notation being $x(i+1/i)$. In the same way (7.26) and (7.24) are rewritten as

$$\bar{\mathbf{w}}(i) = L\bar{e}(i) = L\big(y(i) - \hat{x}(i)\big)$$
$$u(i) = -\hat{d}(i) = -\hat{x}_{d1}(i) \quad . \tag{7.28}$$
$$a = d(i) - \hat{d}(i) + w_0(i) - d_a(i)$$

where the 'bar' denotes estimation, as oppose to prediction since $\bar{e}(i)$ depends on the present $y(i)$. An alternative, but heavier notation is $e(i/i)$.

Remarks. Distinction between $x(i)$ and $\hat{x}(i)$ is essential: the former is an a priori class of signals, model-based, constraint by command and noise class; the latter is a realization of the previous class, what actually occurred. Since realization is driven by the plant measurement $y(i)$, it may be significantly perturbed by discrepancies between plant and EM, with the result of including component outside of the model class! This is the source of feedback control oddities and pitfalls!

One-step prediction $\hat{x}_{d1}(i+1)$ which is available at step i, allows to compute $u(i+1)$ in advance, and to save it, prior of dispatching at the onset of step $i+1$.

Figure 9 shows the block-diagram of the control unit. Thruster dispatching and inversion are lacking, as well digitization and conversions.

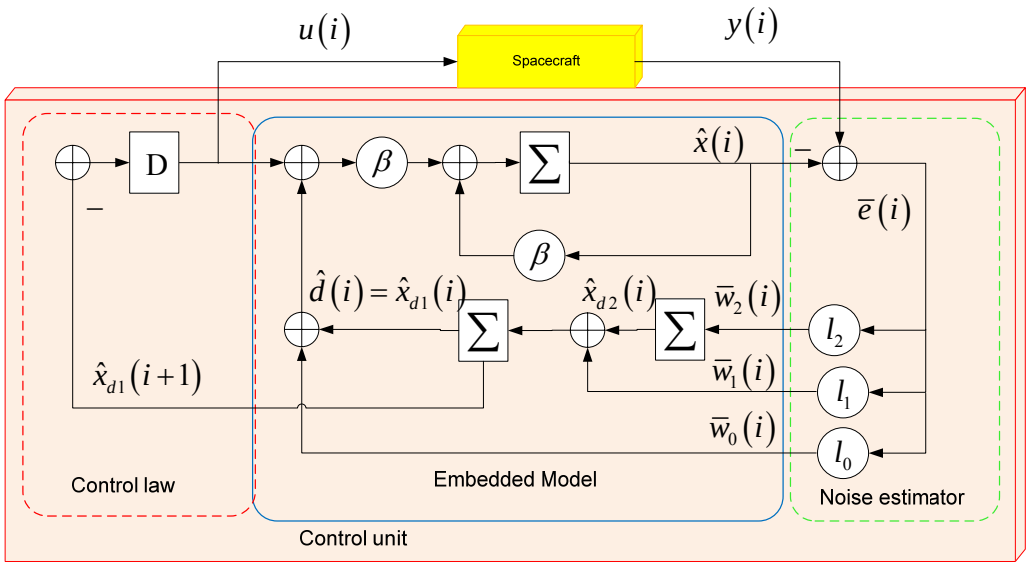

Figure 9. Block-diagram of the control unit, made by embedded model, noise estimator and control law.

1.2.5 Predictor properties

1.2.5.1 Predictor transfer functions

It is worthwhile to convert predictor equation (7.27) into $\mathcal{Z}$ transfer function. To this end, separate controllable transform from (7.16)

$$\begin{aligned} y_m(z) &= M(z)(d + w_0 + u)(z) \\ M(z) &= \beta(z - 1 + \beta)^{-1} \end{aligned} \tag{7.29}$$

and (multivariate) disturbance transform from (7.22)

$$\begin{aligned} d(z) &= \mathbf{D}(z)\begin{bmatrix} w_1 \\ w_2 \end{bmatrix}(z) \\ \mathbf{D}(z) &= \begin{bmatrix} (z-1)^{-1} & (z-1)^{-2} \end{bmatrix} \end{aligned} \tag{7.30}$$

Then the predictor equation from command and measurement to model output holds

$$\begin{aligned} \hat{y}_m(z) &= M(z)\left(u(z) + \left(H_d(z) + l_0\right)(y - \hat{y}_m)(z)\right) \\ \hat{y}_m(z) &= S_m(z)M(z)u(z) + \left(1 - S_m(z)\right)y(z) \end{aligned}, \tag{7.31}$$

where predictor sensitivity S_m is defined by

$$S_m(z) = \left(1 + M(z)\left(H_d(z) + l_0\right)\right)^{-1}$$
$$H_d(z) = \mathbf{D}(z)\begin{bmatrix} l_1 \\ l_2 \end{bmatrix} = (z-1)^{-2}\left((z-1)l_1 + l_2\right) \quad . \tag{7.32}$$

Equation (7.32) allows to make explicit sensitivity and its complement $V_m = 1 - S_m$

$$S_m(z) = \frac{(z-1)^2(z-1+\beta)}{(z-1)^2(z-1+\beta) + \beta l_0(z-1)^2 + \beta l_1(z-1) + \beta l_2}$$
$$V_m(z) = \frac{\beta l_0(z-1)^2 + \beta l_1(z-1) + \beta l_2}{(z-1)^2(z-1+\beta) + \beta l_0(z-1)^2 + \beta l_1(z-1) + \beta l_2} \quad . \tag{7.33}$$

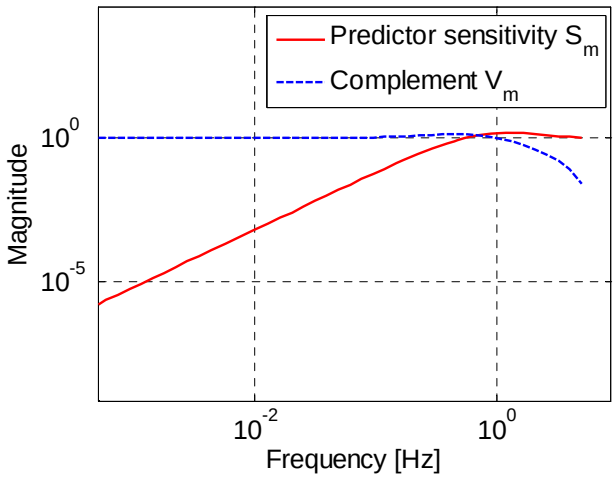

Figure 10. Typical magnitude of drag-free predictor sensitivity and its complement.

1.2.5.2 Predictor gain equation

First the predictor gain equations are given, relating eigenvalues to gain vector L. Then eigenvalues are tuned to requirements.

Write the characteristic equation of the state matrix in (7.27), using the notation $\gamma = \lambda - 1$, which provides

$$P(\gamma = \lambda - 1) = \det\begin{bmatrix} \lambda - 1 + \beta + \beta l_0 & -\beta & 0 \\ l_1 & \lambda - 1 & -1 \\ l_2 & 0 & \lambda - 1 \end{bmatrix} = \gamma^3 + (\beta + \beta l_0)\gamma^2 + \beta l_1 \gamma + \beta l_2 \,. \tag{7.34}$$

Fixing three closed-loop eigenvalues $\Lambda = \{\lambda_k = 1 - \gamma_k, k = 0,1,2\}$, establishes the characteristic polynomial coefficients and the gain equations

$$
\begin{aligned}
&P(\gamma = \lambda - 1) = \gamma^3 + c_2\gamma^2 + c_1\gamma + c_0 \\
&c_0 = \gamma_0\gamma_1\gamma_2 = \beta l_2 \\
&c_1 = \gamma_0\gamma_1 + \gamma_0\gamma_2 + \gamma_1\gamma_2 = \beta l_1 \\
&c_2 = \gamma_0 + \gamma_1 + \gamma_2 = \beta + \beta l_0
\end{aligned}
\qquad (7.35)
$$

*1.2.6 Performance **

1.2.6.1 Residual acceleration equation

Consider the simplified block-diagram of the plant model and control unit in Figure 11.

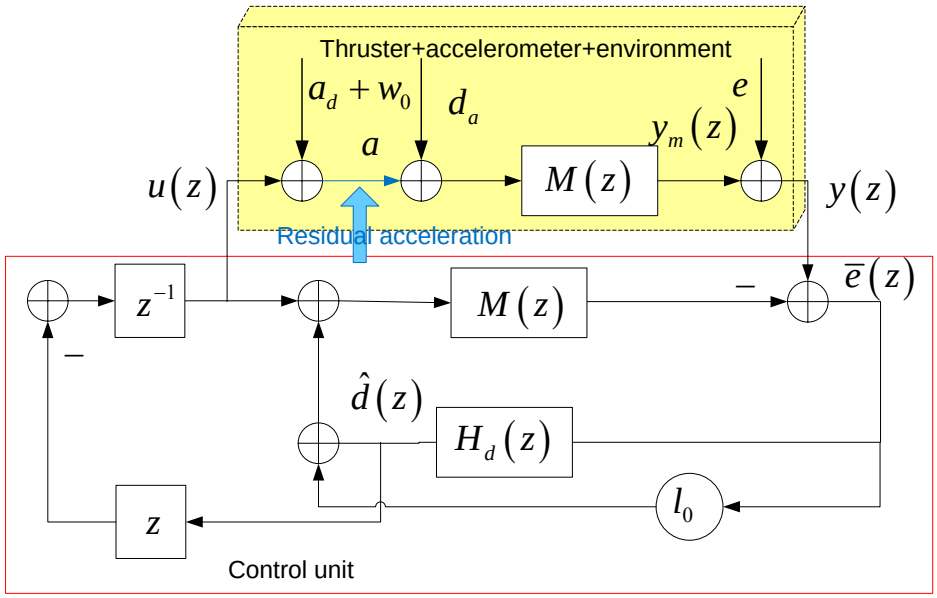

Figure 11. Overall block diagram.

Eigenvalues (and gains) are designed to force residual acceleration to meet requirements, which implies frequency domain. To this end compute the $\mathcal{I}$ transfer function from non gravitational acceleration to residual acceleration.

Rewrite residual acceleration from (7.16) and (7.25) as

$$a = d - \hat{d} + w_0 - d_a \qquad (7.36)$$

where prediction error $\hat{e}_{d1} = x_{d1} - \hat{x}_{d1}$ has been added.

Theorem 1. The actual model error. $\bar{e} = y - \hat{y}_m$ is the output of a dynamic system having transfer function the state-predictor sensitivity $S_m(z)$ and forced by the sum of the output disturbance d_y and model error e.

Proof. Start from predictor output equation (7.31) and write the 'actual' model error

$$\begin{aligned}(y-\hat{y}_m)(z) &= y(z)-M(z)\big(u(z)+\big(H_d(z)+l_0\big)(y-\hat{y}_m)(z)\big)\\ \overline{e}(z) &= S_m(z)\big(y(z)-M(z)u(z)\big)\end{aligned}. \qquad (7.37)$$

The input signal $y(z)-M(z)u(z)$ is the sum of output disturbance and model error since from (7.16) and (7.29)

$$y(z)-M(z)u(z)=M(z)(d+w_0)(z)+e(z)=d_y(z)+e(z). \qquad (7.38)$$

Remarks. Theorem 1. is very generic as it may be applied to any state predictor.

One can now compute the residual acceleration. To this end one should distinguish between environment disturbance ('drag') including thruster noise a_d+w_0 and the measurement noise $e_a=e+M(z)d_a$, which includes also model discrepancies.

Theorem 2. Residual acceleration. It is a combination of environment and measurement noise through the closed loop sensitivity $S=S_m\big(1+l_0M(z)\big)$.

Proof. Start from the definition of a in (7.28) and employ (7.37)

$$a(z)=d(z)+w_0(z)-H_d(z)S_m(z)\big(d_y+e\big)(z)-d_a(z). \qquad (7.39)$$

Rearranging (7.39) and separating d into a_d and d_a, one obtains

$$a(z)=\big(1-M(z)H_d(z)S_m(z)\big)(a_d+w_0)(z)-M(z)H_d(z)S_m(z)\big(d_a+M^{-1}(z)e\big)(z). \qquad (7.40)$$

Now it is straightforward to rewrite the transfer functions in (7.40) as

$$a(z)=S(z)(a_d+w_0)(z)-\big(1-S(z)\big)\big(d_a+M^{-1}(z)e\big)(z). \qquad (7.41)$$

Remarks. Theorem 2. has been obtained in the discrete-time domain. It may be converted into continuous-time domain, by approximating $a(t)$ as a stepwise signal obtained by zero-order-hold (ZOH) reconstructing the sampled values $a(iT)$, which is acceptable as soon as the signal PSD is limited band. In terms of transfer function it holds

$$a(s)\cong Z(s)a\big(z=e^{sT}\big)=Z(s)a^*(s). \qquad (7.42)$$

Remarks. Equation (7.41) clarifies the drag-free trade-off: (i) non-gravitational disturbance are attenuated in the sensitivity BW, from DC to f_m to be designed, as sensitivity is a high-pass filter; (ii) measurement noise and model discrepancies are attenuated outside the sensitivity BW, $f>f_m$, due to high-frequency roll-off of the complement $1-S(z)$.

1.2.6.2 Sensitivity asymptote and BW*

Preliminary is the expression of closed-loop sensitivity, which is slightly different from predictor in (7.33). It holds from (7.33) and (7.40)

$$S(z)=\frac{(z-1)^2(z-1+\beta+\beta l_0)}{(z-1)^2(z-1+\beta)+\beta l_0(z-1)^2+\beta l_1(z-1)+\beta l_2}$$
$$V(z)=\frac{\beta l_1(z-1)+\beta l_2}{(z-1)^2(z-1+\beta)+\beta l_0(z-1)^2+\beta l_1(z-1)+\beta l_2} \quad . \tag{7.43}$$

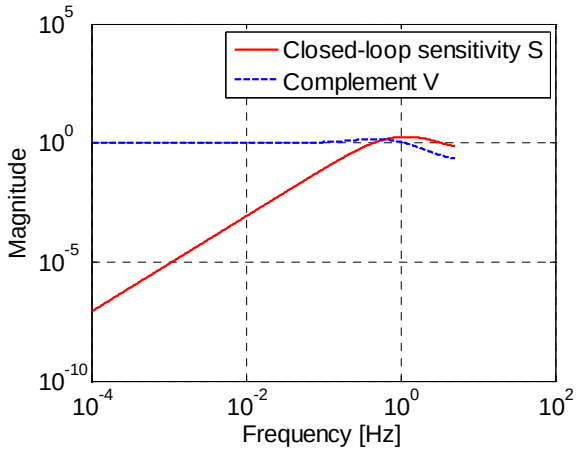

Figure 12. Closed-loop sensitivity and its complement.

A pair of asymptotes are of interest, as they define a cutoff frequency that may be kept as bandwidth. To this end approximate $z-1\cong sT=j2\pi fT$, which is valid as $f<f_{\max}$. Then take the DC limit $f\to 0$ $(z-1\to 0)$ and the high-frequency limit $f\to\infty$ $(z-1\to\infty)$, where the latter is meaningful only when an asymptote exists below $f_{\max}$.

Theorem 3. Sensitivity asymptotes and BW. Taking the above limits yields

$$\lim_{f\to 0} S(jf)=S_0(jf)=\frac{-(2\pi fT)^2}{l_2/(1+l_0)}=-\left(\frac{f}{f_m}\right)^2, \tag{7.44}$$
$$\lim_{f\to\infty} S(jf)=1$$

where the sensitivity BW is defined as

$$f_m=\frac{1}{2\pi T}\sqrt{l_2/(1+l_0)}\,. \tag{7.45}$$

Theorem 4. The complementary asymptotes and BW f_c hold

$$\lim_{f\to 0}\left(1-S(jf)\right)=1$$
$$\lim_{f\to\infty}\left(1-S(jf)\right)=V_\infty(jf)=-\frac{\beta l_1}{(2\pi fT)^2}=-\left(\frac{f_c}{f}\right)^2. \tag{7.46}$$

Remarks. Note sensitivity and complement have different BW as $f_m \neq f_c$.

1.2.6.3 Design degrees-of-freedom and design constraints*

First assume a single degree-of-freedom, setting equal eigenvalues, $\{\gamma_0 = \gamma_1 = \gamma_2\}$, which constrains the BW ratio to be fixed

$$\varphi = \frac{f_c}{f_m} = \sqrt{\frac{\beta l_1 (1 + l_0)}{l_2}} = \sqrt{\frac{3\gamma_0^2 \times 3\gamma_0}{\gamma_0^3}} = 3 . \tag{7.47}$$

To dispose of more freedom, consider two degrees-of-freedom in (7.41): complementary eigenvalues in (7.35) are separated in two sets, i.e. $\{\gamma_0, \gamma_1, \gamma_2 = \gamma_1\}$, which leads to

$$\begin{aligned} \beta l_1 &= \gamma_1 (\gamma_0 + 2\gamma_1) \\ \beta l_2 &= \gamma_0 \gamma_1^2 \\ \beta + \beta l_0 &= 2\gamma_1 + \gamma_0 \end{aligned} . \tag{7.48}$$

Then defining $\gamma = \gamma_1 / \gamma_0$ a 2nd order equation follows

$$\varphi^2 = \frac{(1 + 2\gamma)^2}{\gamma} \Rightarrow \gamma^2 - \gamma(\varphi^2 - 4)/4 + 1/4 = 0 , \tag{7.49}$$

and to the solution

$$\gamma = \frac{1}{8}\left(\varphi^2 - 4 \pm \varphi\sqrt{\varphi^2 - 8}\right), \tag{7.50}$$

which, looking for smaller γ, imposes the BW and eigenvalue constraints

$$\begin{aligned} &\varphi \geq \sqrt{8} \\ &\gamma = \frac{1}{8}\left(\varphi^2 - 4 - \varphi\sqrt{\varphi^2 - 8}\right) \leq 0.5 \end{aligned} . \tag{7.51}$$

thus allowing, in principle, to enlarge the BW ratio. Note γ decreases as φ increases.

It is now possible to play with γ_0 and γ_1 so as to meet requirements.

1.2.6.4 Eigenvalue tuning

The starting equation is the residual acceleration (7.41) which is decomposed in the sensitivity BW, $f < f_m$, and at higher-frequencies, $f > f_c$, under the following simplifying assumptions

1) aerodynamic acceleration a_d dominates in the sensitivity BW, whereas thruster noise w_0 dominates at higher frequencies,
2) accelerometer drift and bias d_a dominates at lower frequencies, whereas e, including the f^2 accelerometer noise dominates at higher frequencies.

Denoting the different spectral densities (root) with S_a, S_d, S_w, S_{da} and S_e one may write

$$\begin{aligned} S_a^2(f) &\cong \left|S_0(jf)\right|^2 S_d^2(f) + S_{da}^2(f),\ f < f_m \\ S_a^2(f) &\cong S_w^2(f) + \left|V_\infty(jf)\right|^2 \left|M_\infty^{-1}(jf)\right| S_e^2(f),\ f < f_c \end{aligned}, \tag{7.52}$$

where, assuming $\beta < 1$,

$$M_\infty^{-1}(jf) = j2\pi fT/\beta, \tag{7.53}$$

whereas under $\beta = 1$

$$\left|M_\infty^{-1}(jf)\right| = 1. \tag{7.54}$$

Now using the aerodynamic spectral density (7.19) and (7.44), the former equation in (7.52) may be rewritten as

$$f_m \geq f_d \sqrt{\frac{S_d^2}{\overline{S}_a^2(f) - S_{da}^2(f)}} \cong f_d \frac{S_d}{\overline{S}_a(f)},\ f < f_m, \tag{7.55}$$

where accelerometer noise (flat) has been assumed negligible wrt to drag-free bound $\overline{S}_a$. Moreover assuming $f_m > f_1$, $\overline{S}_a(f_m) = 5\overline{S}_{a,\min} = 0.1\times 10^{-6}$ m/s$^2/\sqrt{\text{Hz}}$, leads to

$$\begin{aligned} f_m &\geq 5\times 10^{-3} \frac{5\times 10^{-3}}{m \times 0.1\times 10^{-6}} = 0.5 \text{ Hz} = f_{m,\min} \\ S_{da}(f) &<< \overline{S}_a(f),\ f < f_m \end{aligned}, \tag{7.56}$$

which entails $f_c \geq f_{c,\min} = \sqrt{8} f_{m,\min} \cong 1.4$ Hz.

Remarks. Aerodynamic spectral density must account also for thruster drift.

Now denoting $S_e(f) = S_{ah}(f/f_a)^2$, and setting $\beta = 1$, the second equation in (7.52) becomes

$$\begin{aligned} &S_w^2 + S_{aw}^2 (f_c/f_a)^2 \leq \overline{S}_a^2(f),\ f > f_c \\ &f_c \leq f_a \sqrt{\frac{\overline{S}_a^2(f) - S_w^2}{S_{aw}^2}} \end{aligned}, \tag{7.57}$$

where now S_w cannot be neglected due to thruster noise being a critical parameter, as it includes also thruster quantization. Allocating less than half of spectral limit to thruster noise , say $S_w \leq 0.7\overline{S}_{a,\min}$, and assuming $f_a = f_1$ and $S_{aw} < 0.1\overline{S}_{a,\min}$, the following loose limit is obtained

$$\begin{aligned} f_c &\le \frac{0.1}{\sqrt{2}} \frac{\bar{S}_a(f)}{0.1\bar{S}_{a,\min}} \cong 3.5 \text{ Hz} \\ f_c &> f_{c,\min} \end{aligned}, \tag{7.58}$$

close to $f_{\max}$. Actually f_c will be fixed by neglected dynamics.

As a first-stage conclusion, (7.49) leads to

$$\begin{aligned} \gamma_1 &\le 2\pi f_{m,\min} T \cong 0.31 \\ \gamma_0 &\le 2\pi f_{c,\min} T \cong 0.63 \end{aligned}. \tag{7.59}$$

Figure 8 and Figure 9 show the predictor and closed-loop sensitivities under the above design. Sensitivity and complement remain about the same from predictor to closed-loop.

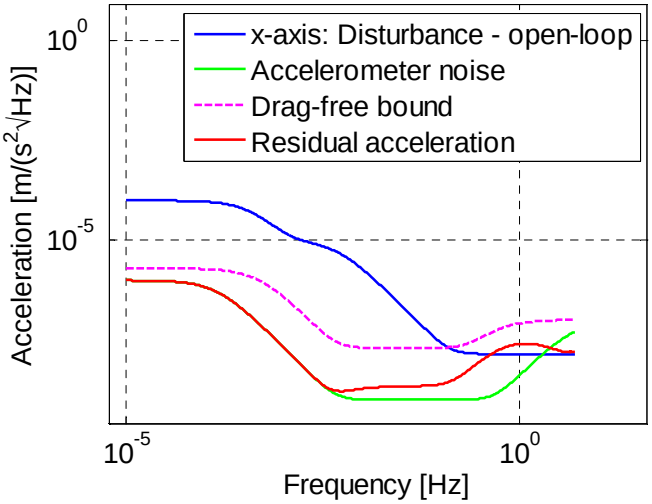

Figure 13. Open-loop disturbance and noise, compared with residual acceleration and drag-free bound.

Figure 10 shows performance are achieved with margin, that may be exploited to either reduce the bound or lower the orbit thus encountering worse aerodynamic forces.

Figure 11 shows the same residual acceleration as in Figure 10, but extended through approximate Laplace transform (7.42) to above $f_{\max} = 5$ Hz. One recognizes the discrete-time PSD repeating periodically, whereas the continuous-time PSD decreases, with zeros at $f = 2kf_{\max}$, due to ZOH reconstruction, whose Fourier transform is the Shannon function.

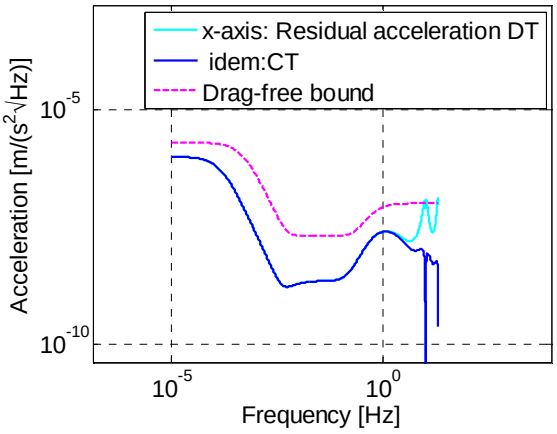

Figure 14. The same performance as above extended above Nyquist frequency.

*1.2.7 Robust stability**

Assume now model error e is due to neglected dynamics. Formulation is done using transfer functions for simplicity's sake. Assume the actual transfer function from a to y, is

$$\begin{aligned} y(z) &= M(z)P(z)a(z) + w_y(z) \\ P(z) &= (1+\partial b)\Delta P(z) \\ \Delta P(z) &= (1+\partial b)z^{-\tau}\sum_{k=1}^{n}\frac{h_k}{z-1+\beta_k},\ \sum_{k=1}^{n}\frac{h_k}{\beta_k}=1 \end{aligned}, \tag{7.60}$$

where w_y is the measurement noise, input independent, and

$$y_m(z) = M(z)a(z). \tag{7.61}$$

Model error is therefore

$$\begin{aligned} e(z) &= (y-y_m)(z) = M(z)\big(P(z)-1\big)a(z) + w_y(z) \\ e(z) &= \big(P(z)-1\big)y_m(z) + w_y(z) = \partial P(z)\,y_m(z) + w_y(z) \end{aligned}, \tag{7.62}$$

where

$$\partial P(z) = (1+\partial b)z^{-\tau}\sum_{k=1}^{n}\frac{h_k}{z-1+\beta_k} - 1. \tag{7.63}$$

is the fractional error dynamics.

Now replacing (7.63) into (7.41) yields

$$\big(1+V(z)\partial P(z)\big)a(z) = S(z)\big(a_d + w_0\big)(z) - V(z)\big(d_a + M^{-1}(z)w_y\big)(z). \tag{7.64}$$

Robust stability is ensured by the circle criterion

$$\max_{|f|<f_{\max}} \left| V(jf)\partial P(jf) \right| \le \eta < 1 \tag{7.65}$$

which places a further constraint to eigenvalues.

Remarks. Note (7.65) maps the model output y_m through the fractional error dynamics to the tracking error of the model output, which is the measured residual acceleration to be kept to zero.

Approximate now $|V(jf)|$ with the high frequency asymptote $(f_c / f)^2$ and

$$\max_f \left| \partial P(jf) \right| = \partial P_{\max} \,@\, f = f_{\partial P}\,. \tag{7.66}$$

Then

$$f_c \le f_{\partial p} \sqrt{\eta / \partial P_{\max}} \le f_{c,\min} = 1.2 \text{ Hz}, \tag{7.67}$$

where the complementary BW limit depending on disturbance rejection has been added. This limit poses a constraint to fractional error dynamics, to be respected for keeping drag-free conditions.

Figure 12 shows $|\partial P(jf)|$ (open-loop) and $|V(jf)\partial P(jf)|$ (closed-loop), under a neglected dynamics composed of a 2nd order thruster dynamics with natural frequency close to 3 Hz and an accelerometer delay of $1.5T$ (50% greater than modeled). The closed-loop (7.65) is neatly below unit, with $\eta < 0.4$, thus leaving margin.

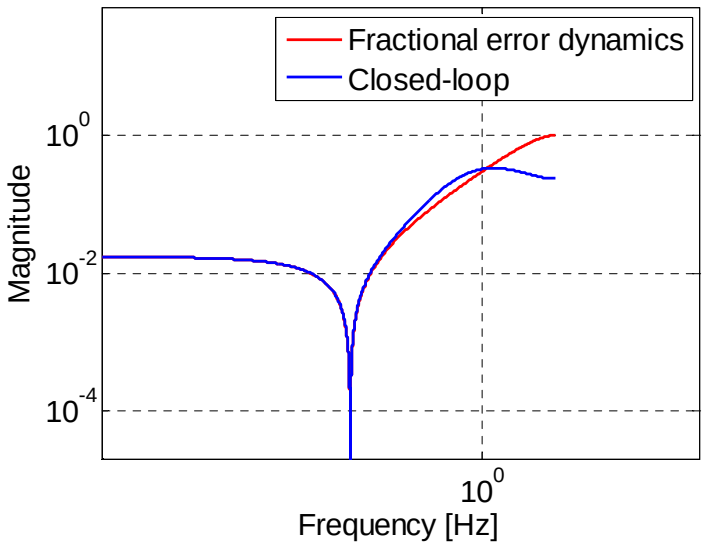

Figure 15. Error dynamics: open and closed-loop.

1.3 Design through sensitivity and complement limits

1.3.1 State equations

To be used in Matlab. We write the state equation of the model as in (7.16)plus the model error

$$\begin{aligned} x(i+1) &= (1-\beta)x(i) + \beta(u + d_u) \\ y(i) &= x(i) + e(i) = y_m(i) + e(i) \\ d_u &= d + w_0 \end{aligned} \tag{7.68}$$

The error model is written as the sum of the measurement noise and of the neglected dynamics as in (7.62), using transfer function

$$e(s) = \partial P(s)\, y_m(s) + w_y(s), \tag{7.69}$$

where

$$\partial P(s) = P(s)/M(s) - 1. \tag{7.70}$$

We assume that the plant is the cascade of an accelerometer delay τ_a and a second order dynamics of the thrusters

$$\begin{aligned} P(s) &= e^{-js\tau_t} \frac{1}{s^2/\omega_t^2 + 2\zeta_t s/\omega_t + 1} \\ \omega_t &= 15 \text{ rad/s} \\ \tau_t &= 1.5T \\ \zeta_t &= 0.7 \end{aligned} \quad . \tag{7.71}$$

The model is a delay of the time unit corresponding to $\beta = 1$

$$M(s) = e^{-jsT}. \tag{7.72}$$

The open-loop magnitude of ∂P is in Figure 15.

The command u is obtained from

$$\begin{aligned} \begin{bmatrix} \hat{x} \\ \hat{x}_{d1} \\ \hat{x}_{d2} \end{bmatrix}(i+1) &= \begin{bmatrix} 1-\beta-\beta l_0 & \beta & 0 \\ -l_1 & 1 & 1 \\ -l_2 & 0 & 1 \end{bmatrix} \begin{bmatrix} \hat{x} \\ \hat{x}_{d1} \\ \hat{x}_{d2} \end{bmatrix}(i) + \begin{bmatrix} \beta \\ 0 \\ 0 \end{bmatrix} u(i) + \begin{bmatrix} \beta l_0 \\ l_1 \\ l_2 \end{bmatrix} y(i) \\ u(i) &= \begin{bmatrix} 0 & -1 & 0 \end{bmatrix} \begin{bmatrix} \hat{x} \\ \hat{x}_{d1} \\ \hat{x}_{d2} \end{bmatrix}(i) \end{aligned} \quad . \tag{7.73}$$

Combining

$$\begin{bmatrix} x \\ \hline \hat{x} \\ \hat{x}_{d1} \\ \hat{x}_{d2} \end{bmatrix}(i+1) = \left[\begin{array}{c|ccc} 1-\beta & 0 & -\beta & 0 \\ \hline \beta l_0 & 1-\beta-\beta l_0 & 0 & 0 \\ l_1 & -l_1 & 1 & 1 \\ l_2 & -l_2 & 1 & 1 \end{array}\right] \begin{bmatrix} x \\ \hline \hat{x} \\ \hat{x}_{d1} \\ \hat{x}_{d2} \end{bmatrix}(i) + \left[\begin{array}{ccc} \beta & \beta & 0 \\ \hline 0 & 0 & \beta l_0 \\ 0 & 0 & l_1 \\ 0 & 0 & l_2 \end{array}\right] \begin{bmatrix} \underline{u}=0 \\ \hline d \\ e \end{bmatrix}(i) \quad . \quad (7.74)$$

$$a(i) = \begin{bmatrix} 0 & 0 & -1 & 0 \end{bmatrix} \begin{bmatrix} x \\ \hline \hat{x} \\ \hat{x}_{d1} \\ \hat{x}_{d2} \end{bmatrix}(i) + \begin{bmatrix} 0 & 1 & 0 \end{bmatrix} \begin{bmatrix} \underline{u}=0 \\ \hline d \\ e \end{bmatrix}(i)$$

Denote the noise estimator gain vector as L.

The DT transfer functions, sensitivity $S(jf) = a/d$, and the complement $V(jf) = 1 - S(jf) = -M(jf)a/e$ are shown below in magnitude.

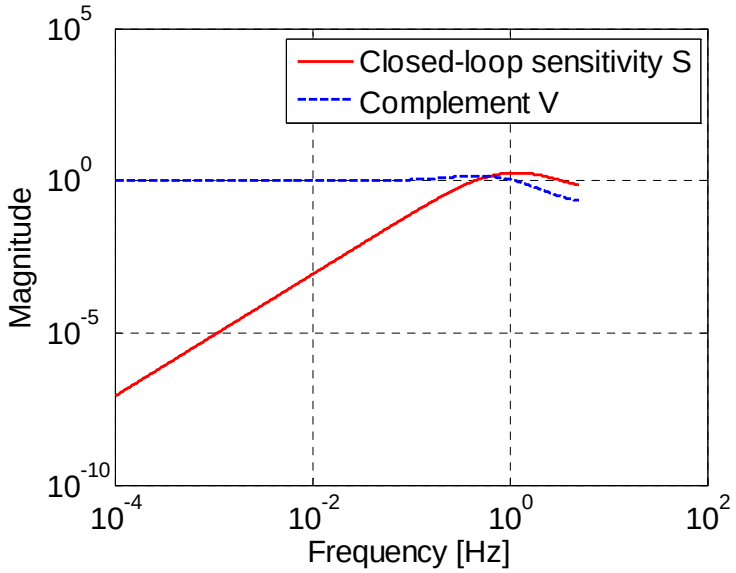

Figure 16. Overall sensitivity and complement.

Clearly

1) the sensitivity (high-pass filter) kills the low frequency of the environment disturbance to be cancelled,
2) the complement is a low-pass filter that kills the high –frequency components of the model error.

1.3.2 Transfer functions

Consider equation (7.41), neglecting d_a

$$a(z) = S(z)d(z) - \left(1 - S(z)\right)M^{-1}e(z). \tag{7.75}$$

relating residual acceleration to environment and model error. Performance of drag-free control is expressed by fixing an upper bound $\bar{S}_a$ to the spectral density S_a of a. Denoting the spectral density of the environment disturbance (including thruster noise) as S_d, and neglecting model error, the following inequality follows

$$\begin{aligned} &\left|S(jf)\right| \le \left|S_d(jf)\right| / \bar{S}_a(jf) = \bar{S}(f) \\ &W_d(jf)\left|S(jf)\right| \le 1 \end{aligned} \tag{7.76}$$

In other words the left hand side expression is an upper limit to the sensitivity magnitude fixed by performance and disturbance class. The upper bound can be also inverted and shifted to right hand side becoming a weighting function.

Now consider the version (7.64)of equation (7.41) including the neglected dynamics

$$\left(1 + V(z)\partial P(z)\right)a(z) \cong S(z)\left(a_d + w_0\right)(z). \tag{7.77}$$

Closed loop stability is guaranteed from (7.65) if

$$\begin{aligned} &\left|V(jf)\right| \le \eta \left|\partial P(jf)\right|^{-1} = \bar{V}(f,\eta) \\ &W_{\partial P}(f,\eta)\left|V(jf)\right| \le 1 \\ &\eta < 1 \end{aligned} \quad . \tag{7.78}$$

The latter is a second inequality relating complement to neglected dynamics.

Figure 17 shows a significant margin exists between limit and sensitivity.

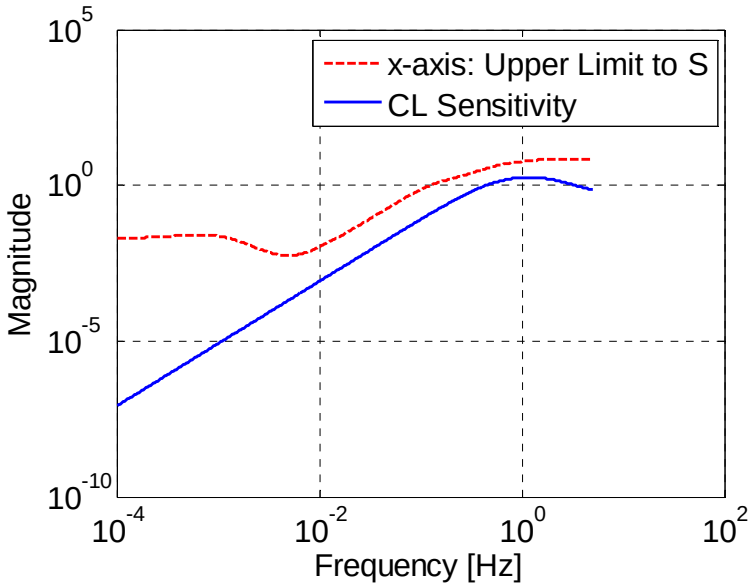

Figure 17. Upper limit and sensitivity.

Figure 18 shows both upper limits and the closed loop transfer functions (magnitude): both have a significant margin.

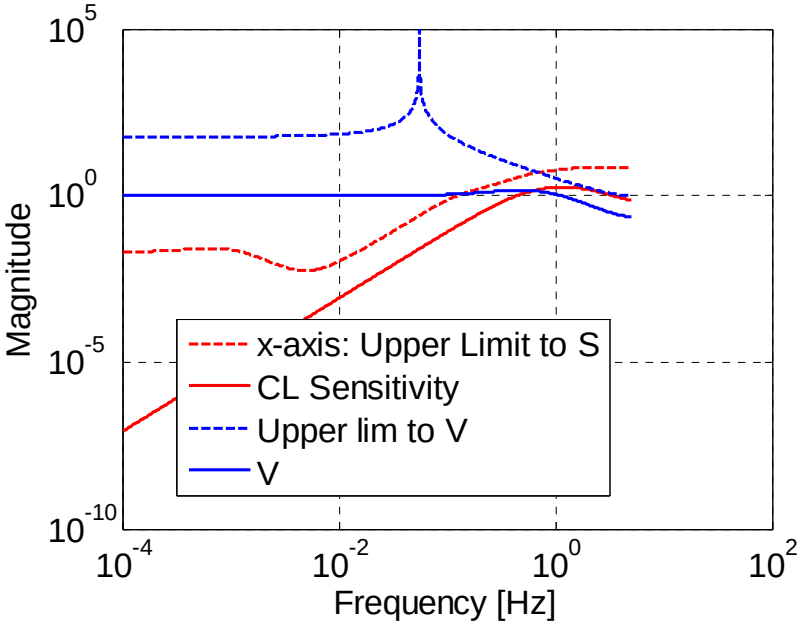

Figure 18. Upper limits to sensitivity and complement.

An approximate design can be done by assuming limits and transfer functions either monotonic increasing or decreasing close to the intersection of the 0 dB axis (crossover

frequencies). The crossover frequencies of $S(f)$ and of $V(f)$ can be approximated by the crossover frequencies f_m and f_c of the low and high frequency asymptotes.

By denoting the crossover frequencies of $\bar{S}$ and $\bar{V}$ with $f_{s,\min}$ and $f_{v,\max}$, one has

$$\begin{aligned} f_m &\geq f_{s,\min} \\ f_c &\leq f_{v,\max}(\eta) \end{aligned}. \tag{7.79}$$

The left hand side of both inequalities (7.76) and (7.78) less than unit can be optimized with respect to design parameter L, trying to minimize their maximum magnitude in the frequency domain.

$$\begin{aligned} L_s^* &= \arg\min_L \max_{|f|\leq f_{\max}} W_d |S| \\ L_v^* &= \arg\min_L \max_{|f|\leq f_{\max}} W_{\partial P} |V| \end{aligned}, \tag{7.80}$$

which provides two results. By using the closed-loop complementary eigenvalues and splitting them into two related sets

$$\gamma_m = \gamma_0 = \gamma_1, \gamma_2 = 2\gamma_m \tag{7.81}$$

(7.80) can be optimized wrt to γ_m, showing that the functional in (7.80) have opposite slope wrt to the argument in the mid frequency domain as shown by Figure 19.

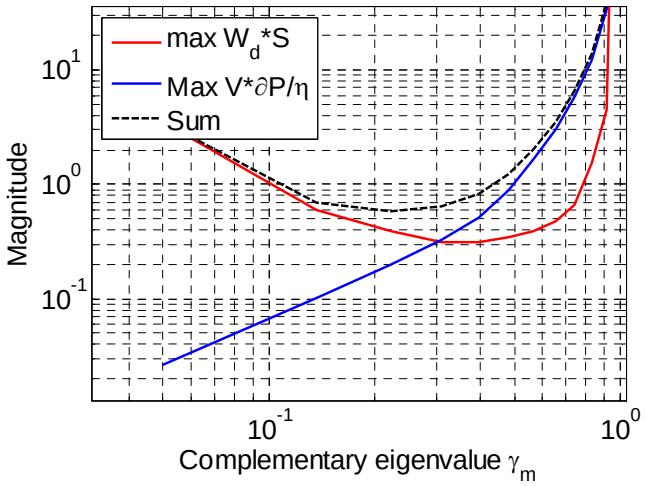

Figure 19. Weighted sensitivity and complement optimized.

Notice how both functions diverge as soon as $\gamma_m \to 1$ (eigenvalue =0), which implies that the state predictor BW cannot be enlarged up to the Nyquist frequency! In fact we are looking for a value of both functional which is less than 1 at the same complementary eigenvalue γ_m. It may be obtained by summing up both functionals (it can be proved the sum has a meaning) as

the convex curve in Figure 19. The resulting optimal eigenvalue for $\eta = 1$ (the largest possible) is

$$\begin{aligned} &\gamma_m^* \cong 0.22 \\ &f_m^* = \gamma_m^* / (2\pi T) \cong 0.3 \text{ Hz} < f_{\max} = 5 \text{ Hz} \end{aligned} . \tag{7.82}$$

2 References

[1] Staff of the Space Department of the Johns-Hopkins-University Applied Physics Laboratory and Staff of the Guidance and Control Laboratory at Stanford University, A Satellite Freed of All but Gravitational Forces: "TRIAD I", *AIAA J. Spacecraft*, Vol. 11, No. 9, September 1974, pp.637-644.

[2] Aircraft Operations Division "JSC reduced gravity program. User's guide", NASA, Lyndon B. Johnson Space Center, November 2007, AOD 33899, Rev. B.

[3] E. D. Kaplan and C. J. Hegarty eds Understanding GPS. Principles and applications. Artech House, Boston, 2006.

[4] G. F. Franklin, J. D. Powell and M. L. Workman Digital control of dynamic systems, Addison-Wesley, Reading (MA), 1990.

[5] D. T. Greenwood *Principles of dynamics,* Prentice-Hall, Englewood Cliffs, 1965.

[6] J. R. Wertz *Spacecraft attitude determination and control,* D. Reidel Pu. Co. , Dordrecht, 1978

[7] B. Wie *Space vehicle dynamics and control,* AIAA Education Series, AIAA inc, Reston, 1988.

[8] M. J. Sidi *Spacecraft dynamics and control. A practical engineering approach.* Cambridge Univ. Press, 1997.

[9] P. C. Hughes, Peter C., *Spacecraft Attitude Dynamics.* New York, Dover Publications, Inc, 2004.

[10] M. H. Kaplan, *Modern Spacecraft Dynamics & Control.* New York : John Wiley & Sons, 1976.

[11] E. Canuto, *Controlli automatici. Parte II. Controllo digitale,* Celid, Torino, 2002.